Geological Sciences
Honors Thesis

Applications of Unidirectional Flow Models to Lower Crustal Deformation

Ka Yan Semechah Lui

Faculty Thesis Advisor: Eric A. Hetland

Chapter One *

Dynamic Controls on the Depth Sensitivity of Lower Crust Viscosity Inferences Over Tectonic Time Scales

Chapter Two

Inferences of the Lower Crust Viscosity at the Cholame section of the San Andreas Fault

Introduction

Chapter one and two share a similar theme as we are using the same fluid-dynamic system to understand the deformation of the lower crust. Specifically, we use unidirectional Poiseuille flow with both uniform and depth-dependent viscosities to model lower crustal flow. In the first chapter, we examine the lithospheric dynamics of the lower crust in the Tibetan region. Previous studies have inferred depth-independent lower crust viscosities of the region based on topographic gradient of the Tibetan Plateau. Assuming that upper crustal deformation mainly depends on the flux of the lower crustal flow and not on the details of the flow at depth, we consider models of lower crustal flow with depth-dependent viscosity which generate identical channel flux as the uniform viscosity model, and draw connections between the depth-independent viscosity and the equivalent depth-dependent viscosity profiles. In Chapter two, using the same fliud-dynamic model, we examine lower crust deformation under the Cholame section of the San Andreas Fault. With non-volcanic tremors found at the base of the lower crust and occurring parallel to the surface trace of the San Andreas Fault, it is proposed that the San Andreas Fault is extending to the base of the crust and is dipping at depth. Here we evaluate whether the occurrence of NVT on the deep extension of the SAF is consistent with lower crustal flow. We do so by constraining the range of viscosities of the lower crust which would allow a localized fault to exist in the lower crust over a time scale of 1 Myr.

***** *Section 4.1 of Chapter 1 is contributed by Professor Eric A. Hetland. I've retained this section in the thesis so that Chapter 1 is presented as it will appear in published form.*

Dynamic Controls on the Depth Sensitivity of Lower Crust Viscosity Inferences Over Tectonic Time Scales[1]

K.Y. Semechah Lui and Eric A. Hetland

Dept. Geological Sciences, University of Michigan, Ann Arbor, MI, 48109

Abstract

It has been proposed that crustal deformation is a result of material flow in the lower crust over time scales of several million years (tectonic time scale). Pervious studies demonstrated that over these time scales, upper crustal deformation mainly depends on the flux of the lower crustal flow and not on the details of the flow at depth. As temperature increases with depth, the viscosity of the lower crust is expected to decrease. Thus a homogeneous Newtonian viscosity over an assumed homogenous viscous lower crustal channel is merely an apparent viscosity of the crust. In this paper, we consider models of a lower crustal flow with depth-dependent viscosity, in order to draw connections between this apparent viscosity and equivalent depth-dependent viscosity profiles. We find that there is a large range of depth-dependent viscosity profiles that are consistent with an inferred apparent viscosity. Also, the apparent viscosity is in general biased toward the lowest viscosities in the lower crust. Furthermore, the apparent viscosity can be lower than the lowest actual viscosity in the lower crust, if the lower crustal channel is underestimated. We finally consider unidirectional flow

[1]This chapter is to be submitted to *Earth Planet. Sci. Lett.* in April 2011.

in models with nonlinear, depth-denpendent viscosity. We find that very low apparent viscosities are only consistent with either high temperatures or strong stresses driving lower crustal flow.
Keywords:
lower crustal flow, lithospheric dynamics, apparent viscosity

1. Introduction

Several studies have proposed that lower crustal flow drives the deformation of the crust over time scales of several million years, hereafter referred to as "tectonic time scales" (*e.g.*, [1–7]). By linking observations indicative of crustal deformation to lower crustal flow, some of these studies were able to infer an apparent viscosity of the lower crust. Most of these models simplify the crust, for instance by describing the lower crust with a single Newtonian viscosity. The effective viscosity of the lower crust is expected to vary with depth, with a variation up to several orders of magnitude (*e.g.*, [8]). Moreover, the dominant deformation mechanism in the lower crust is likely dislocation creep, and thus the viscosity is non-linear (*e.g.*, [8–10]).

Kruse et al. [2] and Kaufman and Royden [3] demonstrated that any inference of a Newtonian lower crust viscosity is only a proxy for the viscous properties of the lower-most crust. Kruse et al. [2] demonstrated that numerical models with non-linear lower crust viscosities predicted upper crustal deformation over tectonic time scales similar to that predicted in simplified models with a homogeneous Newtonian viscosity. Kaufman and Royden [3] also demonstrated that flow in the lower crust with a depth-dependent, nonlinear viscosity was similar to flow in a lower crustal channel with a homoge-

neous Newtonian viscosity. As a consequence of this similarity, a model-based inference of a uniform Newtonian lower crust viscosity is merely an apparent viscosity of the lower crust [3]. Clark and Royden [4] showed that the evolution of topography is sensitive to the apparent viscosity divided by the cube of the channel thickness. Hence, an apparent Newtonian viscosity in any thickness lower crustal channel can be found by rescaling an inferred apparent viscosity determined over a given channel thickness. Ideally, the thickness of the channel should correspond to the thickness of the lower crust that is significantly flowing, although that thickness is not *a-priori* known. Since the apparent viscosity of the lower crust trades-off with the thickness of the assumed channel, we refer to the channel over which the apparent viscosity was determined as the "apparent channel." While an apparent viscosity in a simplified model of lower crustal flow may be uniquely constrained from observations of upper crust deformation, there may be an infinite collection of depth dependent viscous profiles that are consistent with the observations.

Clark and Royden [4] proposed a model in which unidirectional flow in a 15 km thick lower crustal channel is the driving force for the change in crustal thickness and the evolution of topographic gradient. In their model, crustal deformation depends only on the flux of flow in the lower crustal channel, and not on the details of the flow at depth. The position of the viscous channel in the lower crust was not included in their model, although it it is likely that the channel would be in the lower-most crust where viscosities are expected to be smallest. Based on present topographic gradients in Tibet, Clark and Royden [4] argued for heterogeneity in the apparent lower crust viscosity in Tibet, from 10^{16} Pa·sec under the flat central plateau, to 10^{18} Pa·sec in

the southeast and 10^{21} Pa·sec at the eastern edge of the plateau adjacent to the Sichuan basin. Clark et al. [6] subsequently proposed a more detailed model that included 2D horizontal flow around a rigid barrier approximating the Sichuan basin, and found that the topographic gradient surrounding the Sichuan basin was consistent with a lower crust viscosity of 10^{18} Pa·sec.

A low viscosity of 10^{16}–10^{18} Pa·sec is broadly consistent with magnetotelleuric measurements and seismic reflectivity in Tibet that indicating partial melt and/or fluids present in the lower crust (*e.g.*, [11–15]). However, several studies have questioned the lower crust viscosity being this low (*e.g.*, [16–21]). For instance, Hilley et al. [16, 19] used GPS measurements of interseismic deformation to infer viscosities in the range of 1–200 $\times 10^{19}$ Pa·sec. Complicating the comparison of the two studies, the models of Hilley et al. [16, 19] did not contain a separate lower crust and upper-most mantle, and it is not clear how their single viscosity estimate relates to the viscosity of the lower crust and/or mantle [22].

Here we use dynamic modes of pressure driven unidirectional flow in a 2D channel, with both uniform and depth dependent viscosity, to explore the connection between an apparent lower crust viscosity and models of depth dependent viscosity throughout the lower crust. Specifically, we show that inferred apparent viscosities of the lower crust are consistent with a large range of depth-dependent viscosity profiles of the lower crust. Over tectonic time scales, surface observations of upper crust deformation are only sensitive to the viscous properties in the weakest crust (*i.e.*, with the lowest viscosities), even when stronger regions (*i.e.*, with larger viscosities) participate in lower crustal flow. We illustrate the depth sensitivity of inferences of lower crust

viscosity using the dynamic model proposed by Clark and Royden [4]. We first describe unidirectional flow with depth-dependent viscosity, and second we illustrate our model for the case of an apparent lower crust viscosity of 10^{18} Pa·sec. We end with a brief discussion of these results and the effect of non-linear viscosity in the lower crust.

2. Unidirectional Viscous Flow

Unidirectional flow (u) along an infinite length, 2D channel is governed by

$$\frac{d}{dz}\eta(z)\frac{d}{dz}u(z) = -\frac{dP}{dx} \tag{1}$$

where z is depth, x signifies the along channel direction, $\eta(z)$ is depth-dependent viscosity, and dP/dx is a lateral pressure gradient. In these models, dP/dx is due to lateral changes in topography (i.e., a topographic gradient). For constant viscosity (η_o), the solution to (1) with no-slip boundary conditions at the top and bottom of the channel is

$$u(z) = \frac{1}{2\eta_o}\frac{dP}{dx}\left(z^2 - hz\right) \tag{2}$$

where h is the thickness of the channel. Equation (2) is the well known Poisseuille flow, in which flow is greatest in the middle of the channel.

In Earth materials, viscosity decreases exponentially with increasing temperature ($\eta \propto e^{1/T}$), and as temperature increases with depth, viscosity decreases with depth (*e.g.*, [8–10]). Neglecting a stress-dependence of viscosity, potential material changes, and/or depth variations in water content in the lower crust, the highest viscosity in the lower crust (η_H) will be below the brittle-ductile boundary, and the lowest (η_L) at the Moho. For simplicity, we

initially assume a relatively simple functional form of viscosity given by

$$\eta(z) = Ae^{-z/\zeta} + B \tag{3}$$

where both A and B are functions of η_H and η_L, and ζ is a decay constant (Fig. 1a). It is important to reiterate that with equation (3) we are implicitly assuming that the lower crust composition is homogeneous, and thus that viscosity is only dependent on temperature. We also ignore possible non-linearity in viscosity, and we consider the impact of non-linear viscosity in the Discussion section. An analytic expression for unidirectional pressure driven flow in a lower crust with depth-dependent viscosity can be obtained by solving equation (1) using equation (3) and no-slip boundary conditions at the top and bottom of the channel, which we do using Mathematica. We verified the analytic solution numerically using a discritized multi-layered model, where each layer has uniform viscosity. With depth-dependent viscosity, flow is greater in the lowermost crust where the viscosities are lowest. As expected, models with exponentially decreasing viscosity produce larger flow deeper than in models with constant viscosity (Fig. 1b).

3. Sensitivity of Depth-Dependent Viscosity

In the models of Clark and Royden [4] and Clark et al. [6], the evolution of topographic gradient depends only on the depth-integrated flow, and not on the flow velocities at any particular depth. Therefore, two models with the same channel flux but different viscosity distributions will produce identical topographic gradients. For example, the two flow models in Fig. 1a, one with a constant viscosity (η_o) channel and the other with a depth-dependent

viscosity, have the same channel flux. In general, η_o is greater than η_L but is lower than the average viscosity of the depth-dependent viscosity. Each depth-dependent viscosity profile has a unique apparent viscosity, although each apparent viscosity is not uniquely related to only one realization of a depth-dependent viscosity profile. In other words, there are an infinite number of combinations of η_H, η_L, and ζ which have the same apparent viscosity.

When the viscosity exponentially decreases with depth, the largest flow will be in the lower portion of the channel (Fig. 1b), and thus it might be more appropriate to compare the flow in the depth-dependent viscosity model to that in a homogeneous viscosity model with a smaller channel thickness. As the thickness of a uniform viscosity channel decreases and for a constant pressure gradient, the viscosity of the thinner channel will likewise need to decrease in order to maintain the same depth integrated flow (Fig. 1). Hence, it is possible that if one calculates an apparent viscosity using a uniform viscosity model with a thinner apparent channel than the ductile lower crust, the apparent viscosity may actually be lower than the lowest viscosities in the lower crust.

3.1. Illustration for an Apparent Viscosity of 10^{18} *Pa·sec*

We further explore the concepts presented above, using a 15 km thick apparent channel with apparent viscosity of 10^{18} Pa·sec, with flow driven by a pressure gradient of about 40 Pa/m (equivalent to an elevation decrease of 4 km over a distance of 2500 km). This model is inspired by the preferred model of Clark and Royden [4] for Southeastern margin of the Tibetan Plateau. We first assume that the crust above and below the viscous channel

does not flow in response to the topographic pressure gradient, and we second consider that the entire non-seismogenic crust flows. In both cases we assume the viscosity decreases exponentially with depth according to equation (3), and we consider a large range of depth-dependent viscosities, with η_H varying from 10^{17} to 10^{25} Pa·s, and η_L from 10^{15} to 10^{24} Pa·s, excluding any combinations in which $\eta_H < \eta_L$. For each η_H and η_L combination, we determine a corresponding ζ value such that the depth-integrated flow is identical to the channel flux produced with uniform viscosity of 10^{18} Pa·sec.

3.1.1. Flow restricted to a 15 km lower crust channel

In this first set of models, we consider that the flow is only within a 15 km thick channel. We find a suite of depth-dependent viscosity profiles that generate the identical flux as that in a channel with uniform viscosity of 10^{18} Pa·sec (Fig. 2). In other words, the apparent viscosity of these viscosity profiles is all 10^{18} Pa·sec. We only show viscosity profiles with $\eta_H \leq 10^{24}$ Pa·sec, although there is no upper limit of η_H. On the other hand, the upper limit of η_L is the apparent viscosity of 10^{18} Pa·sec. As above, in all cases, the average viscosity of each depth-dependent profile is larger than the apparent viscosity.

3.1.2. Flow in the entire non-seismogenic crust

In the second set of models, we consider that the entire lower crust below the brittle-ductile transition flows in response to a pressure gradient. We continue to assume that the apparent viscosity of 10^{18} Pa·sec was determined over a uniform viscosity channel 15 km thick. Furthermore, we neglect any depth dependence of the horizontal pressure gradient resulting from variation

of densities in the crust, and we do not consider vertical flow that may result from depressions of the Moho under the plateau. We remark on both of these in the Discussions section.

Our choice of the thickness of the ductile lower crust is based on the inferred thickness of the lower crust in Tibet. The Moho beneath the Tibetan Plateau is approximately 65 to 70 km below the Earth surface, and we assume that the brittle-ductile transition is at the base of the seismogenic upper crust at approximately 20 km at depth (*e.g.*, [11, 13, 15]). We then assume that the ductile lower crust is 40 km thick. While the choice of how much of the crust may be flowing due to topographic pressure gradients depends strongly on the rheology of the entire crust, our main focus here is to demonstrate the range of depth-dependent viscosities that all have the same apparent viscosity. We take 40 km as an upper limit of the lower crustal thickness that would be flowing in response to topographic gradients.

As before, we also find a wide range of depth-dependent viscosity profiles that generate the same channel flux (Fig. 3). We only show viscosity profiles with $\eta_L \geq 10^{16}$ Pa·sec and $\eta_H \leq 10^{24}$ Pa·sec, although there is no lower or upper limit of η_L or η_H, respectively. If the entire 40 km thick ductile lower crust flows in response to the topography induced pressure gradient, then η_L can be as large as $10^{19.2}$ Pa·sec, which is about 15 times larger than the apparent viscosity of 10^{18} Pa·sec. If $\eta_L \leq 10^{18}$ Pa·sec, then $\eta_H \geq 10^{20}$ Pa·sec, whereas if η_L is larger than 10^{18} Pa·sec then η_H may be as low as $10^{19.4}$ Pa·sec (Fig. 3c).

4. Discussion

In the above analysis, we assume a single pressure gradient driving unidirectional flow in a linearly viscous lower crust with a simple decrease in viscosity with depth. We also assume a particular apparent viscosity, motivated by the apparent viscosity inferred in eastern Tibet by Clark and Royden [4] and Clark et al. [6]. Poisseuille flow models with either a uniform or a depth-dependent viscosity depend linearly on the pressure gradient. As long as the pressure gradient is the same in the uniform viscosity and depth-dependent viscosity models, the equivalence in viscosity profiles shown in Figs. 2 and 3 will be the same. Uniform Poisseuille flow depends inversely on the apparent viscosity, and thus the depth-integrated flow also depends inversely on the apparent viscosity. If matched to another apparent viscosity, the equivalent depth-dependent viscosity profiles shown above would be offset by the ratio of the new apparent viscosity and 10^{18} Pa·sec. For example, if we had considered an apparent viscosity of 10^{16} Pa·sec, which is the apparent viscosity in the central region of the Tibetan plateau Clark and Royden [4], then the equivalent depth-dependent viscosity profiles shown in Fig. 2 and 3 would be uniformly 100 times lower viscosity.

We implicitly assume that the lower crust is a homogeneous material, where viscosity variations with depth are due only to increasing temperature. Since we considered a wide range of viscosity profiles, our analysis does not depend on a particular geothermal gradient or material. The geothermal gradient and material that would result in any particular combination of η_L, η_H, and ζ in equation (3) might be implausible in the Earth, and in this paper we do not attempt to use mineralogy or geothermal gradient as

constraints on the equivalent depth-dependent viscosity profiles. If there is material heterogeneity in the lower crust, the viscosity profile may not be approximated by equation (3). For example, if there is a transition from wet quartzite in the mid crust to dry dunite in the lower crust, the depth variation in viscosity would be such that the lowest viscosities might be at the base of the mid-crust quartzite layer (*e.g.*, [23]). We could include such layering of depth-dependent viscosity; however, as our analysis is based on the flow flux in the lower crustal channel, and not on the details of the depth-dependent flow, our main conclusions would not change if the depth distribution of flow was different. The apparent viscosity is biased towards lowest viscosities. If the lowest viscosities were at a shallower depth in the lower crust, then the apparent viscosity would depend most strongly on those values, and would be relatively insensitive to the larger viscosities elsewhere in the lower crust.

We assume that a single lateral pressure gradient drives lower crustal flow, along an infinitely long channel with constant thickness. However, it is probable that crustal thickness will co-vary with topography to maintain isostacy, and thus the lower crust will have variable thickness. Additionally, density variations between a thickened crustal root under high topography and lithospheric mantle under adjacent thinner crust would also affect the distribution of pressure gradients in the lower crust. The result would be that instead of lower crustal flow being unidirectional as we assumed, there may be a contribution of vertical flow, particularly at the edge of the crustal root (*e.g.*, [2, 24]). In models that allow for both vertical and horizontal pressure driven flow, the vertical rates are most important when the lower crust is thinner than about 25 km, and that these models of 2D lower crustal

flow can still be approximated by unidirectional flow [2].

4.1. Non-linearity of viscosity

Deformation in the lower crust is most likely in the dislocation creep regime, and thus viscosity non-linearly depends on both temperature and shear stress (*e.g.*, [8–10]). Linear viscosity in models of crustal deformation over tectonic time scales can approximate non-linear viscosity when the deformation is only sensitive to the flow flux [3]. We consider models with non-linear viscosity in light of our above results, and discuss how models with non-linear viscosity differ from those with simply a prescribed depth-dependent viscosity.

Pressure driven flow in a temperature dependent, non-linear viscous channel can be derived from equation (1) assuming an effective viscosity given by

$$\eta_{\text{eff}} = A^{-1/n} e^{\frac{Q}{nRT(z)}} \left(\frac{1}{2} \frac{du}{dz} \right)^{\frac{1-n}{n}} \tag{4}$$

where R is the universal gas constant, n is the power-law exponent, and A and Q are viscous properties. We use Mathematica to solve for the flow distribution, assuming that $n = 3$ and that temperature increases linearly with depth. In Fig. 4a, we show the non-linear unidirectional flow over a 40 km thick lower crust for two temperature gradients, assuming three sets of viscous properties. The viscous properties in the first model approximate wet Quartzite [9], while in the second two models we arbitrarily decrease A by an order of magnitude, or increase Q by 16% (Table 1). Each flow model is chosen so that the depth-integrated flow is the same as in a model with a 15 km thick channel with a linear Newtonian viscosity of 10^{18} Pa·sec (*i.e.*,

the apparent viscosity of the non-linear models). We choose to illustrate our models with a wet Quartzite rheology so that reasonable geothermal gradients can lead to sufficiently low effective viscosities at depth. In the second two models we permute the viscous parameters in order to generate the same depth-integrated flow with hotter temperatures.

A 15 km thick apparent channel roughly correlates with the depths of the largest flow in the non-linear models. We choose a 40 km thick channel as a conservative choice, in that thinner non-linear viscous channels are equivalent to larger apparent viscosities for given viscous properties and temperature gradients. In other words, if we had assumed a thinner channel, the apparent viscosities over a 15 km apparent channel would be larger for a given pressure gradient. Due primarily to increasing temperature, η_{eff} decreases near-exponentially with depth (Fig. 4a). There is a singularity in η_{eff} in the center of the flow, as the strain-rates go to zero in the plug-like flow. Essentially, in the region around the singularity in η_{eff}, the lower crust appears infinitely viscous as it is flowing uniformly with little shear strains.

For pressure driven unidirectional flow using a temperature-dependent, non-linear viscosity model, the flow is non-linearly related to the pressure gradient (*e.g.*, [3]). As a result, the apparent viscosity of non-linear flow models will increase non-linearly as pressure gradient decreases (Fig. 4b). This non-linear decrease in apparent viscosity is in contrast to the Newtonian models presented above, where the apparent viscosity will decrease linearly with decreasing pressure gradient. The flow is non-linearly related to the temperature profile in the channel, and thus as the vertical temperature gradient increases, the apparent viscosity also increases (Fig. 4b).

4.2. Applicability to the low apparent viscosities of central Tibet

Clark and Royden [4] concluded that the apparent lower crust viscosity under the central regions of the Tibetan plateau was at most 10^{16} Pa·sec. The low inferred viscosity was based on the very low topographic gradients in the plateau. Models of postseismic deformation from earthquakes in the plateau also resolve rather low viscosities, although most viscosity inferences are on order of 10^{18} Pa·sec (*e.g.*, [18, 20]). Based on postseismic deformation measurements over about a year following a smaller earthquake on the Tibetan plateau, Ryder et al. [21] found that the viscosity of the ductile lithosphere was no smaller than 3×10^{17} Pa·sec, and due to the short record of postseismic observations they were not able to further constrain the viscosities. As in the above cases for an apparent viscosity of 10^{18} Pa·sec, if Clark and Royden [4] underestimated the thickness of the crust that is flowing, it may be that their apparent viscosity of 10^{16} Pa·sec is consistent with lower crustal viscosities no lower than about 10^{17} Pa·sec. A viscosity of 10^{17} Pa·sec is still an order of magnitude less than postseismic models of larger earthquakes and using longer postseismic records (*e.g.*, [18, 20]) We note that postseismic models may not have the same sensitivity to viscosities at depth as models of pressure driven flow over tectonic time scales. Transient effects due to increases in stress below the base of the fault following the earthquake will also likely result in effective viscosities over postseismic time-scales different from those over tectonic-time scales (*e.g.*, [25]).

Assuming a wet quartzite rheology of the lower crust, plausible geothermal gradients, and the ductile lower crust being 40 km thick, we find that for the lower crust to have an apparent viscosity of 10^{16} Pa·sec, the pressure

gradient would need to be significantly larger than 100 Pa/m (equivalent to a topographic gradient greater than 4/5000 km/km; Fig. 4b). This is because in order to sufficiently lower the effective viscosities, the flow needs to be driven by a very large pressure gradient. The need for such a large pressure gradient is opposite to the model of Clark and Royden [4], in which a low topographic gradient indicates a low apparent viscosity. The unidirectional pressure driven flow model proposed by Clark and Royden [4] may not be a complete model to explain the lack of substantial topographic gradients in the central plateau.

An apparent viscosity of 10^{16} Pa·sec might be possible with a gentle pressure gradient if the crust was significantly hotter (either with larger geothermal gradient or larger temperatures), or was composed of a much weaker material. For a wet quartzite rheology, we find that the temperature gradient of the crust would need to be about 25°C/km with a pressure gradient of about 40 Pa/m, for the apparent viscosity to be as low as 10^{16} Pa·sec. For a temperature of about 250°C at the brittle-ductile transition, and a 40 km thick ductile lower crust, and gradient of 25°C/km would predict a temperature of 1250°C, well above the solidus temperature of wet quartzite. There are geophysical indications of partial melt in the Tibetan crust (*e.g.*, [11–15]), and xenoliths in northern Tibet show evidence of heating to 1350°C [26].

5. Conclusions

There are several models that seek to explain observations representative of crustal deformation due to lower crustal flow over times scales of

several million years (*e.g.*, [1–7]). In those models, upper crustal deformation depends most strongly on the the total flux of lower crustal flow (*i.e.*, the depth-integrated flow), and not necessarily on the particular distribution of depth-dependent flow [3]. By dynamically linking observations to lower crustal flow, many of those studies constrained an apparent viscosity of the lower crust. We explore the connections between apparent viscosity of the lower crust and equivalent depth-dependent viscosity profiles. We find that the apparent viscosity over these time scales is biased towards the lowest viscosities in the lower crust. Due to this, the viscosities in the lower crust may be much larger than the inferred apparent viscosities. For instance, in a channel with an apparent uniform viscosity of 10^{18} Pa·s, depth-dependent viscosity profiles over that same 15 km thick channel can have a maximum viscosity larger than 10^{18} Pa·s and a minimum as high as 10^{18} Pa·s. If more of the lower crust participates in the flow, then the lowest viscosities in the lower crust might actually be up to an order of magnitude larger than the inferred apparent viscosity. This suggests that the seemingly low apparent viscosity of 10^{18} Pa·sec suggested by Clark and Royden [4] and Clark et al. [6] for eastern Tibetan plateau may be consistent with a depth-dependent viscosity profile, in which the minimum viscosity is up to 10^{19} Pa·sec, if they underestimated the thickness of the lower crustal channel that is significantly flowing due to topographic gradients. Likewise, an apparent viscosity of 10^{16} Pa·sec for the central plateau may be consistent with minimum viscosities in the lower crust of about 10^{17} Pa·sec. This viscosity is close to the lower bound of viscosity inferred by Ryder et al. [21], but is still an order of magnitude below what other studies have suggested for the viscosities in this region

(*e.g.*, [16–20]). Based on non-linear viscous unidirectional flow models with a wet quartzite rheology, an apparent viscosity as low as 10^{16} Pa·sec requires either a very hot lower crust or a strong pressure gradient driving the flow.

model	n	A (Pa^n/s)	Q (1/Jmol)	T_o (°C)	ϕ (°C/km)
A	3	1.388×10^{-22}	120,000	250	12.5
B	3	1.388×10^{-23}	120,000	250	17.9
C	3	1.388×10^{-22}	138,600	250	17.9

Table 1: Viscous and temperature properties in the three non-linear viscous models in Fig. 4. Viscous properties in model A are after the viscous properties for wet quartzite from [9]. T_o is the temperature at the top of the viscous channel, and ϕ is the temperature gradient.

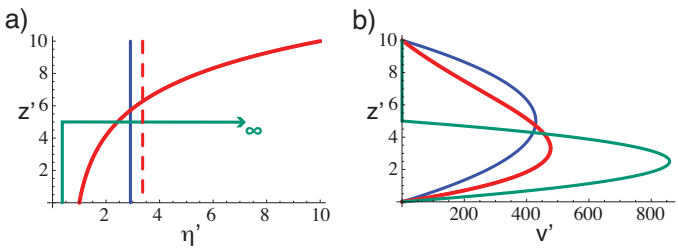

Figure 1: (**a**) Three models of non-dimensional viscosity (η') over a non-dimensional channel thickness (z'): constant viscosity from 0–10 (blue), depth-dependent viscosity from 0–10 (red), and constant viscosity from 0–5 (green). (**b**) The non-dimensional Poisseuille flow (v') corresponding to the viscosity models in (a). All models have the same flux.

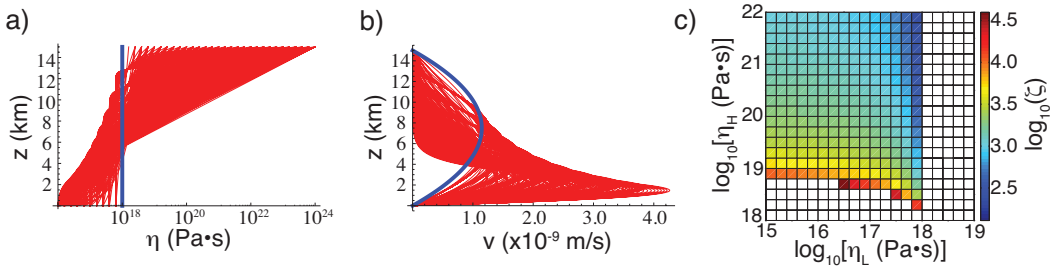

Figure 2: (**a**) Depth-dependent viscosity models (red) all with an apparent viscosity of 10^{18} Pa·sec over a 15 km thick apparent channel (blue). (**b**) Resulting Poisseuille flow for each of the depth-dependent viscosity models in (a; red), and the Poisseuille flow for a uniform viscosity of 10^{18} Pa·sec (blue). (**c**) ζ value required for a depth-dependent viscosity model to have an apparent viscosity of 10^{18} Pa·sec; white region indicates that there is no depth-dependent viscosity model with apparent viscosity of 10^{18} Pa·sec. Solutions are only shown for $\eta_L \geq 10^{15}$ Pa·sec and $\eta_H \leq 10^{22}$ Pa·sec, although there is no lower or upper limit of η_L or η_H, respectively.

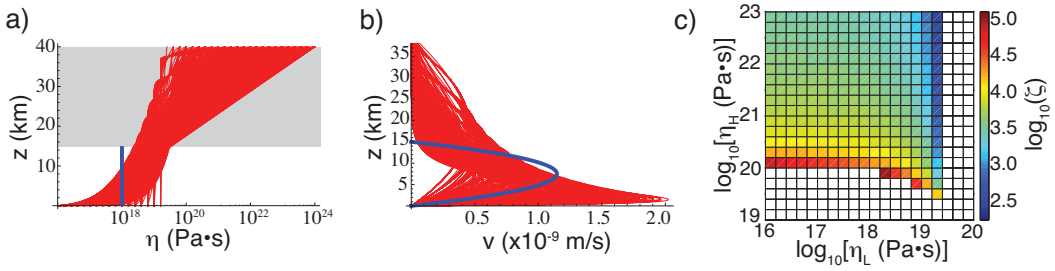

Figure 3: **a**) Depth-dependent viscosity models (red) all with an apparent viscosity of 10^{18} Pa·sec over a 15 km thick apparent channel (blue). (**b**) Resulting Poisseuille flow for each of the depth-dependent viscosity models in (a; red), and the Poisseuille flow for a uniform viscosity of 10^{18} Pa·sec (blue). (**c**) ζ value required for a depth-dependent viscosity model to have an apparent viscosity of 10^{18} Pa·sec; white region indicates that there is no depth-dependent viscosity model with apparent viscosity of 10^{18} Pa·sec. Solutions are only shown for $\eta_L \geq 10^{16}$ Pa·sec and $\eta_H \leq 10^{23}$ Pa·sec, although there is no lower or upper limit of η_L or η_H, respectively.

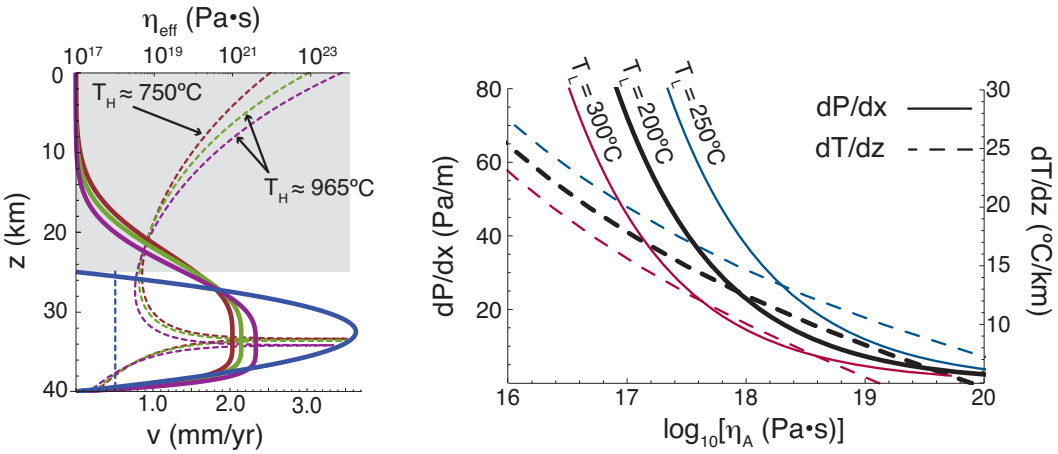

Figure 4: (**a**) Poisseuille flow (solid lines) for a uniform Newtonian viscosity over a channel from 25–40 km depth (blue), and three non-linear viscous models (labelled A, B, and C; see Table 1 for viscous properties and temperatures). The pressure gradient in is 40 Pa/m, and all models have an apparent viscosity of 10^{18} Pa·sec (blue dashed line). Effective viscosity (η_{eff}) of the three non-linear viscous models (colored dashed lines). The temperature at the base of the channel (T_H) is indicated. (**b**) Apparent viscosity of non-linear viscous models as a function of either horizontal pressure gradient (solid lines) or vertical temperature gradient (dashed lines). Models are shown with the temperature at the top of the channel (T_L) either 200°C (blue lines), 250°C (black lines), or 300°C (red lines).

[1] L. Block, L. H. Royden, Core complex geometries and regional scale flow in the lower crust, Tectonics 9 (1990) 557–567.

[2] S. Kruse, M. McNutt, J. Phipps-Morgan, L. Royden, B. Wernicke, Lithospheric extension near lake mead, nevada: A model for ductile flow in the lower crust, J. Geophys. Res. 96 (1991) 4435–4456.

[3] P. S. Kaufman, L. H. Royden, Lower crustal flow in an extensional setting: Constraints from the halloran hills region, eastern mojave desert, california, J. Geophys. Res. 99 (1994) 723–739.

[4] M. Clark, L. Royden, Topographic ooze: Building the eastern margin of tibet by lower crustal flow, Geology 28 (2000) 703–706.

[5] D. McKenzie, F. Nimmo, J. A. Jackson, P. Gans, E. Miller, Characteristics and consequences of flow in the lower crust, J. Geophys. Res. 105 (2000) 11,029–11,046.

[6] M. K. Clark, J. W. Bush, L. H. Royden, Dynamic topography produced by lower crustal flow against rheological strength heterogeneities bordering the tibetan plateau, Geophys. J. Int. 162 (2005) 575–590.

[7] K. L. Cook, L. H. Royden, The role of crustal strength variations in shaping orogenic plateaus, with application to tibet, J. Geophys. Res. 113 (2008) doi: 10.1029/2007JB005457.

[8] D. Kohlstedt, B. Evans, S. Mackwell, Strength of the lithosphere: Constraints imposed by laboratory experiments, J. Geophys. Res. 100 (1995) 587–602.

[9] A. Kronenberg, J. Tullis, Flow strengths of quartz aggregates: grain size and pressure effects due to hydrolytic weakening, J. Geophys. Res. 89 (1984) 4298–4312.

[10] G. Hirth, C. Teyssier, W. J. Dunlap, An evaluation of quartzite flow laws based on comparisons between experimentally and naturally deformed rocks, Int. J. Earth Sci. 90 (2001) 77–87.

[11] L. Brown, W. Zhao, K. Nelson, M. Hauck, D. Alsdorf, A. Ross, M. Cogan, M. Clark, X. Liu, J. Che, Bright spots, structure and magmatism in southern tabet from indepth seismic reflection profiling, Science 274 (1996) 1688–1690.

[12] K. Nelson, W. Zhao, L. Brown, J. Kuo, J. Che, X. Liu, S. Klemperer, Y. Makovsky, R. Meissner, J. Mechie, R. Kind, F. Wenzel, J. Ni, J. Nabelek, C. Leshou, H. Tan, W. Wei, A. Jones, J. Booker, M. Unsworth, W. Kidd, M. Hauck, D. Alsdorf, A. Ross, M. Cogan, C. Wu, E. Sandvol, M. Edwards, Partially molten middle crust beneath southern tibet: Synthesis of project indepth results, Science 274 (1996) 1684–1688.

[13] T. J. Owens, G. Zandt, Implications of crustal property variations for models of tibetan plateau evolution, Nature 387 (1997) 37–43.

[14] W. Wei, M. Unsworth, A. Jones, J. Booker, H. Tan, D. Nelson, L. Chen, S. Li, K. Solon, P. Bedrosian, S. Jin, M. Deng, J. Ledo, B. R. Davi Kay, Detection of widespread fluids in the tibetan crust by magnetotelluric studies, Science 192 (2001) 716–718.

[15] J. Mechie, S. Sobolev, L. Ratschbacher, A. Babeyko, G. Bock, A. Jones, K. Nelson, K. Solon, L. Brown, W. Zhao, Precise temperature estimation in the tibetan crust from seismic detection of the α-β quartz transition, Geology 32 (2004) 601–604.

[16] G. E. Hilley, R. Brgmann, P.-Z. Zhang, P. Molnar, Bayesian inference of plastosphere viscosities near the kunlun fault, northern tibet, Geophys. Res. Lett. 32 (2005) doi: 10.1029/2004GL021658.

[17] B. Meade, Present-day kinematics at the india-asia collision zone, Geology 35 (2007) 81–84.

[18] I. Ryder, B. Parsons, T. Wright, G. Funning, Postseismic motion following the 1997 manyi (tibet) earthquake: Insar observations and modeling, J. Geophys. Res. 169 (2007) 1009–1027.

[19] G. E. Hilley, K. M. Johnson, M. Wang, Z.-K. Shen, R. Brgmann, Earthquake-cycle deformation and fault sip rates in northern tibet, Geology 37 (2009) 31–34.

[20] C. Zhang, J. Cao, Y. Shi, Studying the viscosity of lower crust of qinghai-tibet plateau according to post-seismic deformation, Science in China Series D: Earth Sciences 53 (2009) 411–419.

[21] I. Ryder, R. Burgmann, J. Sun, Tandem afterslip on connected fault planes following the 2008 nima-gaize (tibet) earthquake, J. Geophys. Res. 115 (2010) doi: 10.1029/2009JB006423.

[22] E. Hetland, B. Hager, The effects of rheological layering on postseismic and interseismic deformation, Geophys. J. Int. 166 (2006) 272–292.

[23] J. Jackson, Faulting, flow, and the strength of the continental lithosphere, Int. Geol. Rev. 44 (2002) 39–61.

[24] L. Royden, Coupling and decoupling of crust and mantle in convergent orogens: Implications for strain partitioning in the crust, J. Geophys. Res. 101 (1996) 679–705.

[25] A. M. Freed, R. Roland Burgmann, E. Calais, J. Freymueller, Stress-dependent power-law flow in the upper mantle following the 2002 denali, alaska, earthquake, Earth Planet. Sci. Lett. 252 (2006) 481–489.

[26] B. Hacker, E. Gnos, L. Ratschbacher, M. Grove, M. McWilliams, S. Sobolev, J. Wan, Z. Wu, Hot and dry deep crustal xenoliths from tibet, Science 287 (2000) 2463–2466.

Inferences of the Lower Crust Viscosity at the San Andreas Fault[1]

K.Y. Semechah Lui and Eric A. Hetland

Dept. Geological Sciences, University of Michigan, Ann Arbor, MI, 48109

Abstract

Under the Cholame section of the San Andreas Fault (SAF), non-volcanic tremors (NVT) have been observed at a depth of 26 km below the Earth surface. The tremors occur along a linear trace parallel to the surface trace of the SAF, and are likely to reflect shear slip on the lower crustal fault shear zone. The tremor indicates that the SAF extends to the base of the crust and is dipping at depth. Here we test whether the occurrence of NVT on the deep extension of the SAF is consistent with lower crustal flow. Assuming a fault perpendicular pressure gradient of 100 Pa/m, we find that if the lower crust is a uniform viscosity greater than 10^{20} Pa·s, then the perturbation to a lower crust fault or shear-zone would be less than 1 km laterally. If we consider viscosity to be depth-dependent, minimum viscosity in the lower crust can be less than 10^{20} Pa·s, but only in the lower part of the flow channel. We also evaluate the effect of differential velocity between the upper crust and the uppermost mantle, and find that only a very low differential velocity is consistent with a small fault perturbation.

[1]This chapter is to be submitted to *Geophys. Res. Lett.* in July 2011.

Keywords:
non-volcanic tremors, lower crustal flow, lateral fault perturbation,
Newtonian viscosity, differential velocity

1. Introduction

The Cholame section of the San Andreas fault (SAF), which belongs to the central part of the SAF, has a brittle-ductile transition (BDT) inferred at a depth of 15 to 20 km (*e.g.*, [1]). Below this depth, crustal materials are inferred to deform plastically with the presence of high temperature (*e.g.*, [2–4]). Since energy is unable to accumulate, seismic events are commonly assumed to be absent.

Recent studies indicate that non-volcanic tremors (NVT) are present under the Cholame section of the SAF at a depth of 26 km [5]. This depth is approximately 10 km below the deepest regular earthquakes on the fault. The NVT occur in a near-linear structure in map view, slightly eastward at the SAF, but striking parallel to the fault, within a width of 1 km. The NVT are likely to be reflecting shear slip on the lower crustal fault shear zone, similar to as in subduction zone tremor. Shelly et al. [5] therefore propose that the SAF may extend to the base of the crust, and that the NVT are occurring on the deep extension of the SAF. The fact that the NVT are located only slightly to the east of the surface trace of the SAF suggests that the SAF is dipping at depth.

The presence of the deep NVT presents several questions regarding the dynamics of the non-seismogenic region. Here we focus on whether the occurrence of NVT on the deep extension of the SAF is inconsistent with lower

crustal flow. Specifically we investigate whether flow in the lower crust will lead to perturbation of the fault, and if so, by what extent. In other words, with the indication that lower crust faults exist, we seek to constrain the range of viscosities of the lower crust which would allow a localized fault to exist in the lower crust over a time scale of 1 Myr. We use pressure-driven unidirectional flow in a 2D channel and consider only flow perpendicular to the SAF. We argue that topographic gradient evolves depending only on the depth-integrated flow, and not on the flow velocities at any particular depth (*e.g.*, [6, 7]). In this study, we evaluate separately both uniform and depth dependent viscosity models. A channel with uniform viscosity is the simplest case, in which flow is the largest in the center of the channel. A uniform viscosity is, nonetheless, not geophysically reasonable, as lower crust viscosity is expected to decrease with depth due to a temperature change (*e.g.*, [2, 3, 8]). It is more plausible to assume that viscosity is depth-dependent. In this case, we expect the flow distribution to vary much more significantly. As temperature increases with depth, viscosity is expected to be the lowest at the base of the channel. Thus crustal flow is believed to concentrate in the lowermost part of the crust, where the maximum flow velocity is also assumed to occur. Furthermore, we consider the effect of differential velocity between the upper mantle and the upper crust. In the following, we describe three simple models of lower crustal flow and apply them to investigate the stability of a fault on shear zone in the lower crust over 1 Myr. We end with a brief discussion and conclusion.

2. Modeling equations

2.1. Uniform Viscosity

Unidirectional flow (u) along a 2D channel with infinite length is governed by

$$\frac{d}{dz}\eta(z)\frac{d}{dz}u(z) = -\frac{dP}{dx} \tag{1}$$

where z is depth, x signifies the along channel direction, $u(z)$ is viscosity as a function of depth, and $\frac{dP}{dx}$ is the lateral pressure gradient. In these models, $\frac{dP}{dx}$ is approximated based on changes in topography (i.e., lateral topographic gradient). Assuming that $u(z)$ equals a constant value (η_o) and solving with no-slip boundary conditions at the top and bottom of the channel, the solution to Equation (1) is

$$u(z) = \frac{1}{2\eta_o}\frac{dP}{dx}\left(z^2 - hz\right), \tag{2}$$

where h is the thickness of the channel. Equation (2) is the well-known Poisseuille flow, in which the maximum flow occurs in the middle of the channel.

2.2. Depth-dependent Viscosity

Assuming that the lower crust is homogeneous and that variation of viscosity with depth is due only to temperature. For simplicity, we approximate the viscosity in the lower crust by

$$\eta(z) = Ae^{-z/\zeta} + B, \tag{3}$$

where both A and B are functions of maximum viscosity (η_H), minimum viscosity (η_L) , and ζ is a decay constant. Note that by using Equation (3)

to describe viscosities in the lower crust, we do not attempt to constrain viscosity profiles based on rock deformation experiments. Rather we seek to find plausible distributions of viscosities in the lower crust that lead to small perturbation of a lower crustal fault perpendicular to the SAF. Using the same no-slip boundary condition as above, we use Equation (1) and (3) to obtain an analytic expression for unidirectional pressure driven flow in the lower crust.

2.3. Differential velocity between the uppermost mantle and the upper crust

In the third model, we take into account a differential velocity between the uppermost mantle and the upper crust to account for a potential coupling of the upper mantle and upper crust. With constant viscosity (η_o), the flow is also governed by Equation (1) but with a different boundary conditions u(0) = 0 and u(z) = u_o. The solution in this case is

$$u(z) = \frac{1}{2\eta_o}\frac{dP}{dx}\left(z^2 - hz\right) + u_o\frac{z}{h} \tag{4}$$

The velocity of the base of the lower crust (u_o) can be either positive or negative, depending on the direction of mantle motion relative to the pressure gradient driving the Poiseuille flow in the lower crust (*Fig.1*). Equation (4) is simply the addition of Poiseuille and Couette flow.

3. Illustration for the lower crust beneath the San Andreas Fault

The average crustal thickness in Southern Californian is approximately 30 km (*e.g.* [1, 9]). The depth of the brittle-ductile transition is inferred to be at about 15 km based on seismicity observations. For simplicity, our studies involve a constant pressure gradient perpendicular to the SAF. By primitive

approximation, there is a decrease of 600 m in elevation over a lateral distance of 330 km from the Basin and Range to near the SAF region. Therefore, we take a lateral pressure gradient in the neighborhood of 100 Pa/m to be a conservation reference value. We assume that only fault-perpendicular flow perturbs the pattern of the fault. Hence at the depth where maximum flow is found, we also expect that the maximum finite offset is

$$\delta = uT \tag{5}$$

where T is the timescale over which lower crust flow will perturb a lower crustal fault or shear zone. Here we arbitrarily use $T = 1$ Myr. Since Shelly et al. [5] observe the localized deformations to span a width of ≤ 1 km away from the surface trace of the SAF, we consider models of lower crustal flow of ≤ 1 km to be plausible.

4. Results

When testing models with uniform viscosity, we consider lower crustal flow assuming a wide range of viscosities with $\frac{dP}{dx} = 100$ Pa/m and $T = 1$ Myr. As flow is inversely proportional to a uniform viscosity, fault perturbation decreases with increasing viscosity (*Fig.2*). For a perturbation less than 1 km, we find that viscosity values have a lower limit of approximately 10^{20} Pa·s, but do not have an upper limit.

When considering depth-dependent viscosities, we use the same $\frac{dP}{dx}$ and T. Our models are based on a large range of η_H and η_L, and ζ, excluding any η_H-η_L combinations in which $\eta_H \geq \eta_L$. In general, maximum fault perturbation decreases with increasing η_L values. For all the models with

fault perturbation within a magnitude of 1 km, the position of the maximum offset is biased toward the lower half of the flow channel (*Fig.3*). Among the models tested that have fault offset of less than 1 km. η_L can be as low as 10^{16} Pa·s, but in this case η_H needs to be larger than 10^{21} Pa·s (*Fig.4*). Given a 15-km thick channel, if we consider lower crust viscosity to be depth-dependent, it is possible to find $\eta(z) \leq 10^{20}$ Pa·s over the lowermost 8,500 m of the lower crust (*Fig.5*).

For simplification, we only consider a lower crust with uniform viscosity in the case of differential velocity between the upper crust and the uppermost mantle, using the same $\frac{dP}{dx}$ and T. As mentioned in *Section 2.3*, the velocity of mantle can be either positive or negative depending on the direction of motion. In this case, we find that if the differential velocity exceed 1.5 mm/yr, fault perturbation perpendicular to the SAF will exceed 1 km. We also find that if the differential velocity is opposite of the $\frac{dP}{dx}$ flow, the minimum of the lower crust viscosity can be $\leq 10^{20}$, but only very slightly at $10^{19.8}$ Pa·s (*Fig.6*).

5. Discussion

In the uniform viscosity models, we found that the lower crust viscosity needs to be larger than 10^{20} Pa·s in order for fault perpendicular flow not to have offset a lower crust fault for more than 1 km laterally. This lower limit of viscosity depends on the choice of $\frac{dP}{dx}$ and time scale over which we consider the fault to be perturbed. We assume a lateral pressure gradient of 100 Pa/m in our study, which is fairly high. Poiseuille flow is linearly related to $\frac{dP}{dx}$, so a drop in pressure gradient to 10 Pa/m will reduce the lower bound

of viscosity by an order of magnitude (*Fig.2*). Similarly, the length of time scale (T) over which the lower crustal flow perturbs the SAF is also unclear. There is an inverse linear relationship between T and the magnitude of fault offset. For a longer time period of 2 Myr, the fault offset will be doubled with the same viscosity. In other words, as T increases by two times, the lower limit of viscosity is approximately $10^{20.3}$ Pa·s, which is doubled the viscosity value when T is 1 Myr (*Fig.2*). Therefore, the absolute limit of lower crust viscosity can vary depending on how we determine the other parameters in the equation, but it can be easily found by simple scaling.

Based on the assumption that crustal deformation depends on the flow flux in the lower crust and not the flow distribution at depth, there is a wide range of depth-dependent viscosities that is consistent with an inferred apparent viscosity [10, 11]). However, among these depth-dependent viscosities, crustal flow distribation can vary significantly, depending on η_H and η_L at the channel boundary, as well as how the viscosity is decaying with depth (ζ in Equation (3)). In other words, for a given crustal flow with a uniform viscosity at η_o and maximum flow velocity at V_o, if we are to generate another crustal flow with identical flow flux but with depth-dependent viscosities instead, such crustal flow can have a maximum flow velocity of up to twice the magnitude of V_o. Hence the estimation of the extent of lower crust fault perturbation can vary significantly depending on the viscosity model chosen to evaluate the lower crustal flow.

In *section 4*, we illustrate that for a fault offset of less than 1 km, the maximum differential shear motion (v_o) between the upper crust and the uppermost mantle cannot exceed 1.5 mm/yr. We include this differential

velocity to approximate cases of which the upper crust is weakly coupled to the uppermost mantle (i.e. with upper crust moving at a different rate than the mantle.) If the upper crust is strongly coupled to the underlying mantle, the differential velocity will be less than with weak coupling. 1.5 mm/yr indicates strong coupling of the uppermost mantle and the upper crust. It is important to note that at $v_o \leq 1.5$ mm/yr, the maximum fault offset is expected to be at the base of the lower crust. Such constant shear will result in merely a 2° dip of a originally vertical fault or shear zone. Thus this is still consistent with our understanding to the geometry of the SAF.

6. Conclusion

The discovery that non-volcanic tremors occur in the lower crust under the SAF, and are almost parallel to the trace of the SAF, have led to the suggestion that the SAF extends to the base of the crust as a discrete fault or narrow shear zone [5]. The fact that the SAF extends throughout the lower crust can be argued as a distinct shear plane, the lower crust is flowing due to loaded pressure, and only the effect of fault-perpendicular flow is considered, we evaluate the ranges of possible lower crust viscosities which are consistent with the observed deformations. Considering only fault-perpendicular lower crustal flow over a 1-Myr time scale and assuming a channel with uniform viscosity driven by a pressure gradient of 100 Pa/m, we find that as long as the viscosity of the lower crust is larger than 10^{20} Pa·s, fault perturbation will not exceed 1 km. This pressure gradient is equivalent to a decrease in elevation of 600 m over a distance of 330 km, representing a gross topographic gradient from the Basin and Range to the SAF. If the pressure gradient is one

order of magnitude lower, the acceptable viscosity will also be one order of magnitude lower. If we model the lower crust with depth-dependent viscosity, η_L can be as low as 10^{16} Pa·s. Although in this case, η_H cannot fall below 10^{21} Pa·s, and viscosity $\leq 10^{20}$ Pa·s can only occur in the lowermost 8,500 m of the flow channel. We also find that with uniform viscosity, the maximum differential velocity is 1.5 mm/yr if we consider a differential velocity between the upper crust and the uppermost mantle, reflecting possible but small decoupling throughout the lower crust.

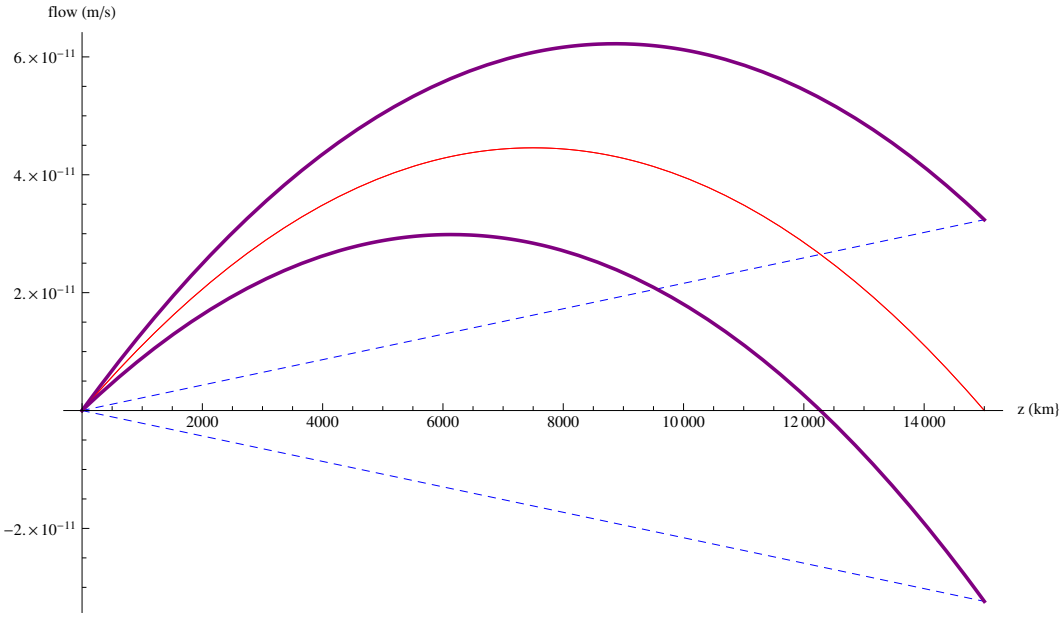

Figure 1: Two possible end-members of the overall flow profiles (purple, solid) in a 15-km lower crust if we consider the effect of a differential velocity between the upper crust and the uppermost mantle. Here we assume two possible directions of mantle flow (blue, dashed) with the unidirectional deformation creep (red) in the lower crust.

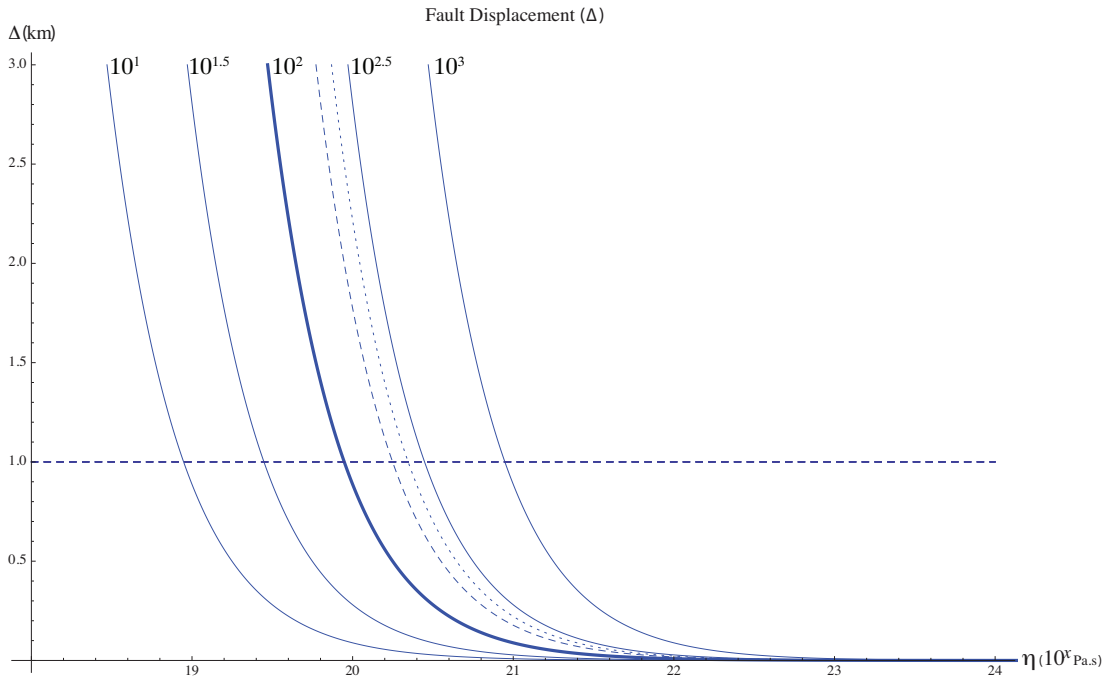

Figure 2: The relationship of uniform viscosity in the lower crust (η) and the magnitude of fault perturbation (δ). Numbering on individual curves are lateral pressure gradients in Pa/m. All solid lines represent displacement (δ) over a time scale of 1 Myr. The dashed and dotted lines indicate displacement under 10^2 Pa/m in 2 Myr and 2.5 Myr respectively.

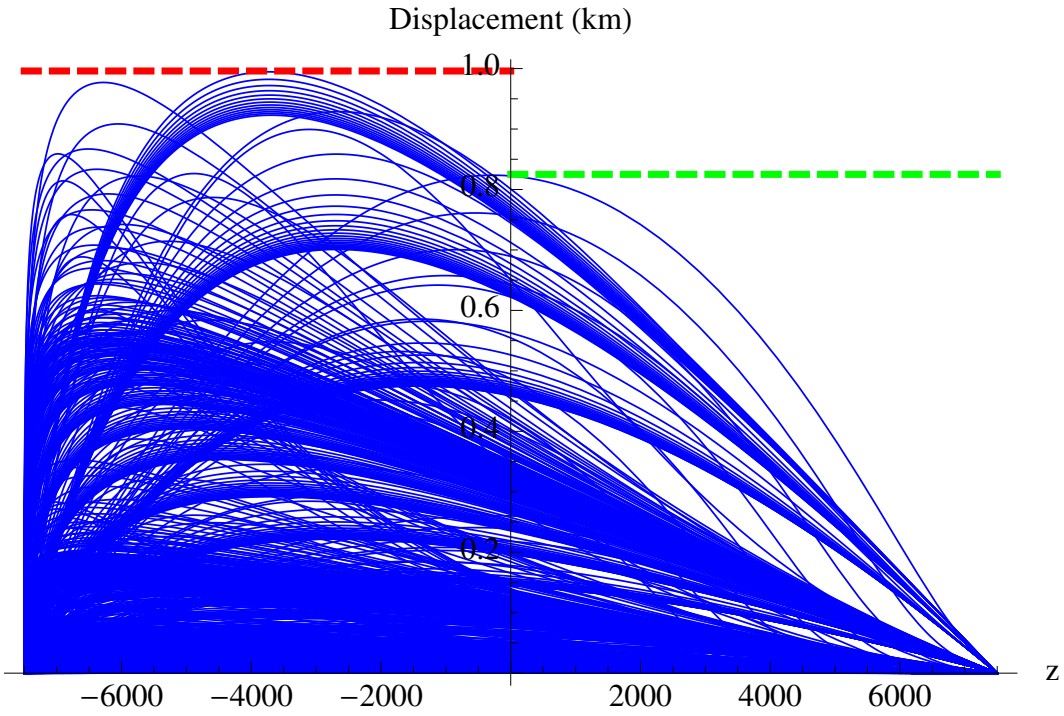

Figure 3: All lower crustal flow profiles corresponding to a range of depth-dependent viscosities. Among all the flow profiles, the maximum fault perturbation is biased toward the lower-half of the flow channel. Considering a 15-km channel, the maximum perturbation in the upper-half is less than 0.8 km, while that in the lower-half can reach as large as 1 km.

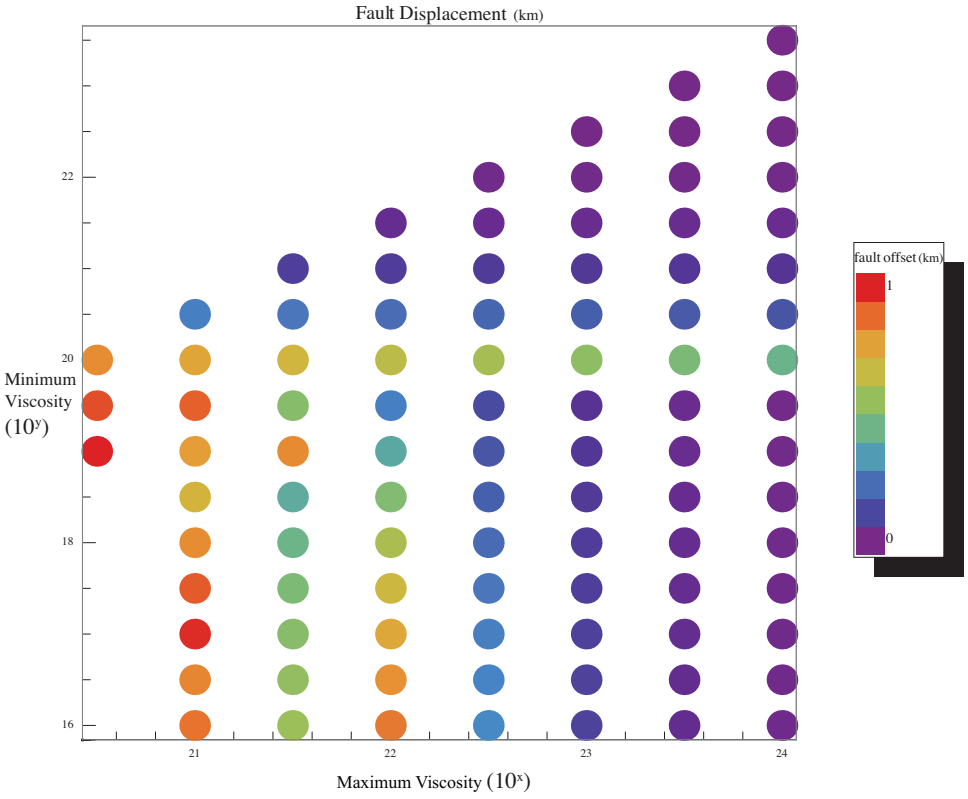

Figure 4: In the case of depth-dependent viscosity, the diagram above shows all combinations of maximum and minimum viscosities (η_H and η_L) in a 15-km flow channel that generate fault perturbation of less than 1 km. The color scale indicates the magnitude of fault displacement in km.

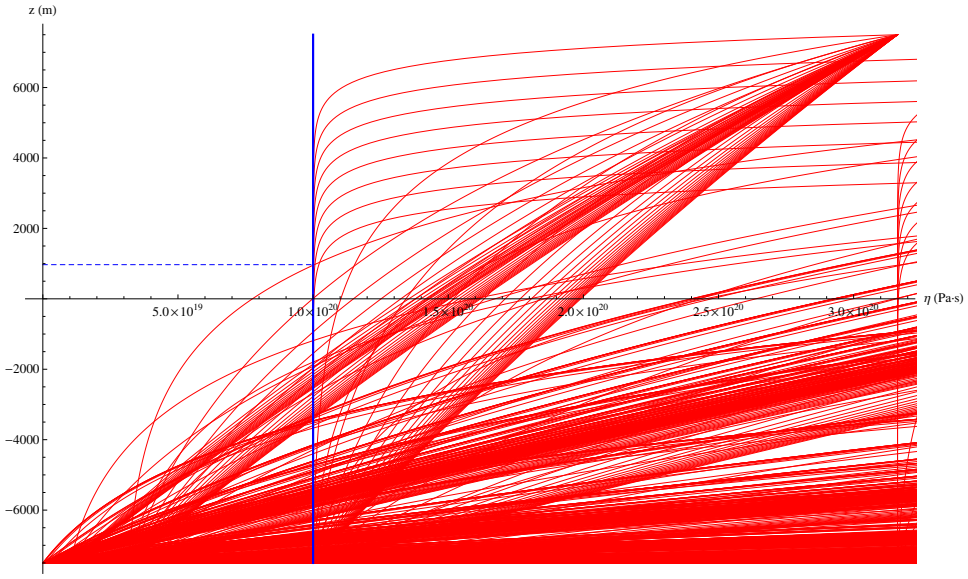

Figure 5: Among the models tested with 10^{16} Pa·s $\geq \eta_L$, $\eta_H \leq 10^{20.5}$ Pa·s (excluding all η_H-η_L combination in which η_H is less than η_L), Fig.5 shows all plausible depth-dependent viscosity profiles which correspond to a channel flow that perturb the fault by less than 1 km. In depth-dependent viscosity models, it is possible for η_L to be $\leq 10^{20}$, but these viscosities can only occur in the lowermost 8,500 m other flow channel.

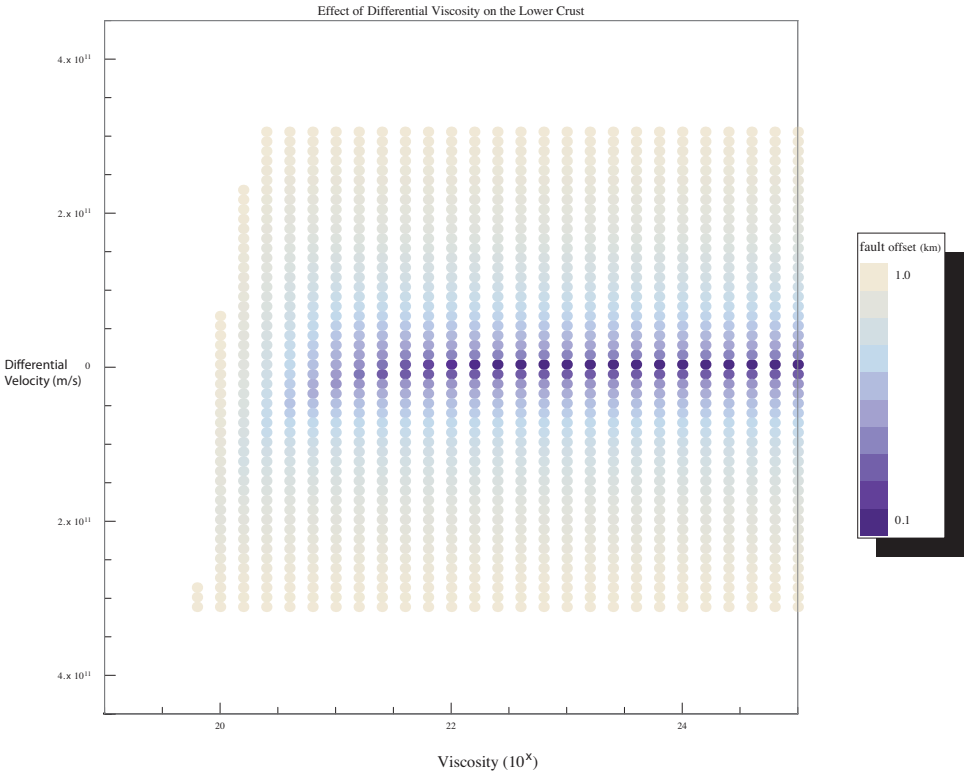

Figure 6: The diagram above illustrates the lower limits of viscosities in a 15-km uniform-viscosity lower crustal flow channel, under the effect of a differential shear motion, ranging from -1.5 mm/yr to 1.5 mm/yr, between the upper crust and the uppermost mantle. The color scale indicates the magnitude of fault displacement in km.

References

[1] J. L. Hardebeck, E. Hauksson, Crustal stress field in southern california and its implications for fault mechanics, J. Geophys. Res. 106 (2001) 21859–21882.

[2] A. Kronenberg, J. Tullis, Flow strengths of quartz aggregates: grain size and pressure effects due to hydrolytic weakening, J. Geophys. Res. 89 (1984) 4298–4312.

[3] D. Kohlstedt, B. Evans, S. Mackwell, Strength of the lithosphere: Constraints imposed by laboratory experiments, J. Geophys. Res. 100 (1995) 587–602.

[4] G. Hirth, C. Teyssier, W. J. Dunlap, An evaluation of quartzite flow laws based on comparisons between experimentally and naturally deformed rocks, Int. J. Earth Sci. 90 (2001) 77–87.

[5] D. R. Shelly, W. L. Ellsworth, T. Ryberg, C. Haberland, G. S. Fuis, J. Murphy, R. M. Nadeau, R. Burgmann, Precise location of san andreas fault tremors near cholame, california using seismometer clusters: Slip on the deep extension of the fault?, Geophys. Res. Lett. 36 (2009) doi: 10.1029/2008GL036367.

[6] M. Clark, L. Royden, Topographic ooze: Building the eastern margin of tibet by lower crustal flow, Geology 28 (2000) 703–706.

[7] M. K. Clark, J. W. Bush, L. H. Royden, Dynamic topography produced by lower crustal flow against rheological strength heterogeneities bordering the tibetan plateau, Geophys. J. Int. 162 (2005) 575–590.

[8] E. Hetland, B. Hager, The effects of rheological layering on postseismic and interseismic deformation, Geophys. J. Int. 166 (2006) 272–292.

[9] L. Zhu, H. Kanamori, Moho depth variation in southern california from teleseismic receiver functions, J. Geophys. Res. 105 (2000) 2969–2980.

[10] P. S. Kaufman, L. H. Royden, Lower crustal flow in an extensional setting: Constraints from the halloran hills region, eastern mojave desert, california, J. Geophys. Res. 99 (1994) 723–739.

[11] K. Y. S. Lui, E. A. Hetland, Dynamic controls on the depth sensitivity of lower crust viscosity inferences over tectonic time scales (in preparation), Earth Planet. Sci. Lett. (2011).